RFID Support for Accurate 3D Localization

Jullawadee Maneesilp, Chong Wang, Hongyi Wu, *Member*, *IEEE*, and
Nian-Feng Tzeng, *Fellow*, *IEEE*

Abstract—This paper pursues RFID support for localization, aiming to pinpoint an object in 3D space. Given a set of RFID tags and/or readers deployed as reference points at known locations in a hexahedron (like shipping container or storage room), a passive and an active localization schemes are considered in this paper. Being the very first range-free 3D localization, our schemes depend solely on RFID tags and readers without other devices or sensors, and it avoids the need of distance estimation according to received wireless signal strength or phase difference. Our passive scheme locates an RFID tag attached to the target object, with both tags and readers as reference points. The active scheme locates an RFID reader, by iteratively determining a 3D sphere best covering the activated reference tags, referred to as the *de*cision *b*oundary optimization scheme (DeB). Results by simulations and testbed experiments using Alien RFID kits have been obtained, and they reveal that DeB outperforms its passive counterpart and achieves the localization error of 0.07 ft. Additionally, DeB yields better location accuracy and yet is much faster than a previous counterpart. With *e*nhanced DeB (EDeB), accuracy of an object located near a hexahedron side or corner is improved considerably.

Index Terms—3D space, antennas, object localization, radio frequency identification (RFID) tags and readers, range-free schemes, spherical models

◆

1 INTRODUCTION

R ADIO frequency identification (RFID) has gained widespread adoption for automatic operation and tracking lately [20], [23]. An RFID system consists of two components, the transponder (or tag) and the detector (or reader). The RFID tags are categorized as either passive or active ones. A passive tag possesses a coupling element and a small, inexpensive electronic microchip, operating without a separate external power source. It is activated only when situated within the interrogation range of a reader, which supplies required power to the transponder through the coupling unit. An active RFID tag, on the other hand, is powered by an internal battery to enable a longer operating range, albeit to a larger size and higher price. Currently, the RFID reader chip can be made very tiny in size, smaller than a US quarter [21]. With low power, such an RFID reader chip is designed to equip portable electronic devices (e.g., smart phones, PDAs, and so on) with RFID technology. It is expected that diverse applications will be developed out of such small sized RFID gear.

Object localization is one of the most important applications of the RFID system to determine the rough trajectory of a moving target or the presence of an object [6], [20], [23]. It is usually realized by deploying RFID tags and/or readers at known positions to compute the possible location of a target object. For example, readers may be deployed in strategic locations in a warehouse or workshop. When an object with an RFID tag passes the reader, the system detects the rough location of the object. Alternatively, if a set of RFID tags are placed at known locations as reference points, a person carrying a portable electronic device with an embedded tiny RFID reader (or a robot equipped with an RFID reader [13], [25], [27]) can obtain rough location information according to the responses of nearby reference tags. While locating RFID tags is better known, positioning RFID readers can gain importance when tiny RFID reader chips are popularly embedded in smart phones (or other portable electronic devices), an expected technological development trend. In particular, given the fact that readers are much more reliable than tags, such positioning technology may be applied for security and safety monitoring. For example, if an individual carrying a smart phone with an embedded RFID reader walks close to a dangerous area (e.g., a radiation or restrictive zone), an alert/alarm will be raised immediately.

The problem of RFID localization on 2D planes has been investigated extensively [4], [13], [14], [15], [17], [19], [22], [25], while increased attention is given to positioning in its 3D counterpart [8], [9], [23]. The localization approaches largely fall into two categories [7]: distance-based (DIS, also known as range-based) and range-free (RAF). A DIS technique is based on estimated distances between transponders (or tags) and detectors (or readers) [10]. Such a technique often suffers from low accuracy in distance estimation due to complex environments and dynamic channel conditions. As a result, two RAF positioning schemes (i.e., a passive and an active ones) are considered here, doing away with distance estimation altogether. Our passive scheme locates an RFID tag, which is attached to the target object, based on a Nelder-Mead nonlinear optimization method to minimize error objective functions using RFID tags and readers deployed as the reference points. It is,

- *J. Maneesilp is with the Pollution Control Department, Ministry of Natural Resources and Environment, Bangkok, 31/8 Soi.19, Ngamwongwan Rd., Bangkrasor, Maung, Nonthaburi 11000, Thailand. E-mail: jullawadee@gmail.com.*
- *C. Wang, H. Wu, and N.-F. Tzeng are with The Center for Advanced Computer Studies (CACS), University of Louisiana (UL) at Lafayette, PO Box 44330, Lafayette, LA 70504-4330. E-mail: chongwang88@gmail.com, wu@cacs.louisiana.edu, tzeng@cacs.louisiana.edu.*

thus, named as the Nelder-Mead nonlinear optimization scheme (first introduced in our prior publication [23]). On the other hand, our active scheme locates an RFID reader, with only RFID tags as the reference points and without other devices or sensors (like video cameras, odometers, built-in distance, angle sensors, and so on, exemplified in [13], [14], [15], [19]) for localization support. It follows an iteration process, dubbed *decision boundary optimization* (DeB), aiming to determine a sphere model, which is the best fit of the activated reference tags such that the sphere center is the estimated target position. Being RAF, our both localization schemes avoid the need of distance estimation according to received wireless signal strength (known to be notoriously inaccurate) [9], [13] or phase difference (being complicated) [3], [5], [8]. Consequently, their accuracy levels are expected to be independent of the types of readers (which often exhibit different radiation patterns). Moreover, our active scheme is less expensive than earlier ones, which rely on localization support of other devices or sensors [13], [14], [15], [19] to achieve desired positioning accuracy, and faster in coordinate calculation than other methods, which call for repeated activation of nearby tags to progressively reach desirable localization accuracy [6], [25], [27].

In this work, we consider a hexahedron space in which target objects are to be localized. We carry out analyses, extensive simulations, and testbed experiments by using the Alien RFID kits [1], [2] to evaluate the proposed localization schemes. Both schemes meet the desired accuracy requirement (i.e., to limit the error of the coordinates to less than 5 percent of the longest edge of the hexahedron) of applications such as 3D packaging and tracking in containers or storage rooms. The errors are mainly due to asymmetric antenna gains, limited radio ranges, significant multipath fading, unreliable signal transmission, irregular coverage by reader's interrogation signals (called coverage irregularity, as also shown in the sensitivity and orientation chart of ALN-9540 Squiggle passive tags [1]), and border/corner effects commonly existing in RFID systems, which together lead to various degrees of false positive reads (that detect tags outside the presumed interrogation range) and false negative reads (that miss tags inside the interrogation range) in RFID systems. To further enhance localization accuracy, we exploit multiple antennas (in contrast to the use of multiple readers or mobile readers), as detailed in Section 3.4. Note that it is common for an RFID reader to support multiple antennas. For example, an Alien Technology's ALR-9900 reader (employed in our testbed experiments) provides four antenna connectors [2]. Moreover, we propose tag compensation to deal with "wall adversary," as to be discussed in Section 5.2.

The rest of this paper is organized as follows: Section 2 discusses related work. Section 3 introduces our proposed passive and active 3D positioning schemes. Simulation and testbed experimental results are presented in Sections 4 and 5, respectively. Finally, Section 6 concludes the paper.

2   RELATED WORK

In tandem with widespread adoption of RFID due to reduced ownership costs, the need of localizing RFID gear rises as well. Location information is usually critical for RFID applications, prompting investigation into different positioning techniques [20], mostly for locating tags. In general, those techniques may be DIS or RAF, where the former relies on distance estimation between a tag and the reader (often making use of received signal strength or phase difference from tags) and the latter counts on tags, which respond upon receiving interrogation signals from the reader. Employing received signal strength [9], [17], a DIS technique is suitable for locating active tags, whose signal strength indications received by the reader can be discriminated. When based on reception phase difference, a DIS technique needs multiple readers/signals [3], [5] or supplemental devices (like pan-tilt units [8]) in additional to RFID gear. Meanwhile, a DIS technique was considered previously [5], where the RFID reader transmits multiple signals with different fundamental frequencies to active tags. A tag then emits backscatter modulated signals, which are received and demodulated by the reader to calculate the distance to the tag based on received signal strength information. The use of phase difference for RFID tag localization has been exploited recently, involving software-defined radio receivers and a pan-tilt unit for experimental evaluation [8]. However, the complexity of algorithms for reception phase calculation is high and an additional pan-tilt unit for accuracy improvement leads to an expensive method. Separately, LocAtioN iDentification based on dynaMic Active Rfid Calibration (LANDMARC) [17] deploys a set of active RFID tags at designated locations as references. It utilizes a small number of readers, each with several transmission power levels. Based on proximity information of detected reference tags, LANDMARC estimates the location of a tracking active tag [17], able to achieve accuracy in the order of a meter only.

In contrast, RAF techniques are applicable to both active and passive RFID tags, with the latter deemed advantageous due to their low costs, long durability, small footprints, and no energy losses. RAF techniques have been explored for wide applications, including autonomous robot navigation and warehouse management [4], [6], [13], [25], [27]. Such a technique employs the RFID reader to activate nearby tags, which report their existence (and perhaps their stored data as well). It can detect the target tags within the reader's interrogation signal ranges (of more than 30 feet for ALN-9540 Squiggle tags [1], based on our measurement). When the RFID reader is attached to an autonomous robot for navigation, RAF techniques can be followed to enhance location information [6] by detecting its nearby reference tags placed inside a building, able to greatly lower the time needed for global localization of the mobile robot. Similarly, mobile robot self-localization was achieved using an RFID reader mounted on the robot to scan the prearranged tags with the support vector machine scheme [27]. The preceding two cases [6], [27] consider the localization of readers carried by mobile robots. Another RAF technique localizes passive RFID tags by utilizing the characteristic curves of tag reads and writes at different signal attenuation levels and at different distances [25]. In addition, several recent studies on mobile robot localization relied on the use of RAF techniques together with other devices or on-robot sensors (like video cameras, odometers, built-in distance, angle sensors, and so on) to achieve better positioning accuracy [14], [15], [19]. Note that all known RAF techniques (except for our prior work [23]) are for 2D localization.

In wireless sensor network (WSN) systems, location information with coarse accuracy is sufficient for most applications. Therefore, several RAF localization approaches have been proposed [7], [10] as cost-effective alternatives to expensive range-based approaches. The RAF techniques in WSN also perform well under random node placement and irregular signal pattern. Separately, effort has been placed on localization and positioning in general wireless networks [15], aiming to guide routing and facilitate information gathering. For example, a self-configurable positioning mechanism for multihop wireless networks was treated earlier [26]. The Cricket Location Support System [18] and the Active Badge Location System [24] have been developed by employing ultrasonic technology to provide location information. Like RAF techniques, all those localization mechanisms for wireless and sensor networks, however, are limited to 2D localization systems.

2.1 Earlier Nelder-Mead Localization (NeM) Scheme

An earlier localization scheme has been treated in [23], where Nelder-Mead nonlinear optimization is followed to minimize the error objective functions, called the NeM scheme. In such a scheme, the reader situated inside a 3D hexahedron activates part of the reference tags placed at known positions on the ceiling and the floor planes [23]. NeM first builds two circles (one on each plane) to approximate the shapes of the activated tags in 2D, before finding the radius and the center of each circle via nonlinear optimization. The x and y coordinates of the RFID reader are estimated using the center points of the two circles. Each circle center is at a point whose distances to chosen activated tags are as close to one another as possible, obtained by minimizing the distance variation function. In other words, NeM carries out distance optimization over a 2D plane first (to get the circle center according to chosen tags on the plane, be the ceiling or floor plane), deemed as the 2D optimization phase (outlined next). Once the centers on both planes are obtained, the z coordinate of the reader can be calculated accordingly. Different approaches toward choosing reference tags for coordinate calculation are studied, including the Inner border method (IBM), Full border method (FBM), and Solid circle method (SCM) [23].

A Simplex method is employed to find the center (x_f, y_f, 0) and radius r_f of the circle formed by the chosen set of reference tags (depend on the chosen methods, i.e., IBM, FBM, and SCM) on the floor. Then, an error objective function is defined, and the Nelder-Mead Simplex optimization is then followed to minimize the defined error objective function. The center (x_c, y_c, 0) and radius r_c of the circle on the ceiling can be derived similarly. Then, x and y coordinates of the reader are determined by averaging (x_f, y_f) and (x_c, y_c), and the z coordinate is obtained from r_f, r_c, and the height of the hexahedron. This earlier considered NeM scheme will be compared with the schemes proposed here in Sections 4 and 5.

3 PROPOSED 3D LOCALIZATION SCHEMES

We propose two RFID-based 3D localization schemes, namely, a passive scheme and an active scheme discussed in the following sections. The proposed schemes are for locating an object with reference to a predetermined arbitrary coordinate system. They are RAF, employing RFID gear alone without additional devices or sensors. Without loss of generality, we consider a hexahedron space (like a shipping container, a storage room, or other hexahedron-shaped spaces), whose length, width, and height are L, W, and H, respectively.

In the rest of this section, we first discuss the challenges and our main contributions. Our passive and active localization schemes are then described in sequence, followed by discussion on accuracy improvement for our active localization.

3.1 Challenges and Contributions

The basic idea of localization in RFID systems is to employ reference points to help determine the position of the target. For example, to locate an RFID reader, reference tags must be deployed in the system. Based on the responses from them, the coordinates of the reader can be derived.

Earlier work [6], [11], [20] is mostly built upon simplified system models. For example, the wireless signal propagation is usually assumed ideal, such that the RFID reader can communicate with any tag within a perfect sphere centered at the reader and with a radius equal to its standard interrogation range. Such assumptions greatly simplify the complexity of localization. However, our preliminary experiments have revealed that they do not hold in a real environment, leading to challenges summarized below:

- Due to the asymmetric antenna gain and multipath fading, signal transmission from the reader does not form a perfect sphere (see Fig. 6, for example). Without this assumption, straightforward geometric calculation cannot be applied.
- It becomes more challenging when the reader operates near a side/corner or other obstructions, where only partial and irregular responses from reference tags can be obtained (as shown in Fig. 11c).
- Communication in RFID systems exhibits low reliability even under static environments. Tags do not always respond to reader scanning, leading to unexpected "holes" often observed in our experiments (as depicted in Fig. 11).

3.2 Passive Scheme

The proposed passive scheme aims to locate an RFID tag, which is attached to the target object, using RFID tags and readers as reference points with known coordinates. The Nelder-Mead nonlinear optimization scheme is employed to minimize the error objective functions. Although its initial setup cost is high due to the need of a set of RFID readers as reference points, the passive scheme is capable of localizing multiple targets simultaneously, especially suitable for tracking inexpensive target objects in a small space for delay-insensitive applications.

3.2.1 Localization System Description

The passive scheme for 3D localization is illustrated in Fig. 1, where the reference tags with known coordinates are placed only on the ceiling (or the floor) of the hexahedron.[1]

---

1. Note that this is the minimum requirement. One may deploy more reference tags on other sides of the hexahedron to enhance accuracy.
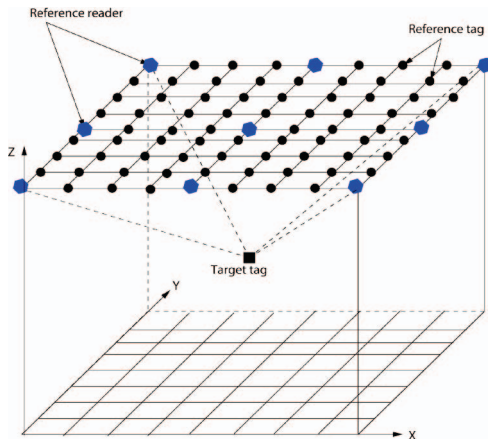
Fig. 1. Three-dimensional passive positioning scheme.

In addition to the reference tags, $N(\geq 4)$ RFID readers are deployed on the ceiling (usually at the vertices or edges). As to be discussed later, deploying more readers may increase accuracy, but result in a longer computing time and a higher cost. The passive scheme requires the readers with multiple transmission power levels. Here, each RFID reader is assumed to have K transmission power levels, which are calibrated so that there is a linearly increasing response range with the increase of power level. The reference tags and readers are placed appropriately with their accurate coordinates stored either in the tags and/or readers or in a database maintained by a local server.

3.2.2 Tag Coordinate Calculation

Upon receiving the request for locating one (or multiple) RFID tag(s), all readers scan the target tag(s) and report the gathered information of activated tags to a computer for coordinate calculation. More specifically, the readers start with the lowest power level and gradually increase the transmission power until they receive the response from the target tag.[2] At the same time, each reader also receives the responses from reference tags. Let Φ_k denote the set of RFID tags which send responses when the reader uses power level k. Let us consider a reader i and a target tag j. If $j \notin \Phi_k$ and $j \in \Phi_{k+1}$, the distance between i and j, denoted by L_{ij}, can be estimated by averaging the distances from the reader to all reference tags that are in Φ_{k+1} but not in Φ_k. After a set of approximate distances from the target tag j to the N readers, i.e., L_{1j}, $L_{2j} \ldots$, $L_{ij} \ldots L_{Nj}$ are collected, the location of the tag j is determined by minimizing the error function using the Nelder-Mead nonlinear optimization, which is defined as

$$\varepsilon = \sum_{i=1}^{N} \left(\frac{L_{ij} - \hat{L}_{ij}}{L_{ij}} \right)^2. \qquad (1)$$

Here, (x_i, y_i, z_i) and (x_j, y_j, z_j) denote the coordinates of reader i and target tag j, respectively. Thus, the distance from reader i to the tracking tag j is represented by

$$\hat{L}_{ij} = \sqrt{(x_i - x_j)^2 + (y_i - y_j)^2 + (z_i - z_j)^2}. \qquad (2)$$

---

2. Linear search is employed here for the illustrative purpose. Fast search methods (such as binary search) may be employed to improve efficiency.
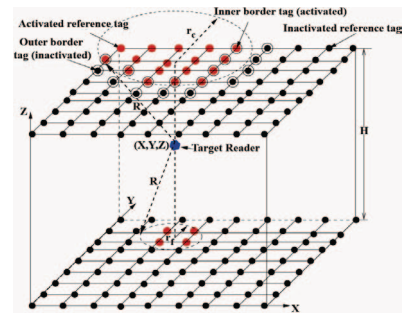

Fig. 2. Three-dimensional positioning scheme.

The Simplex method [16] is used for minimizing the error objective function ε to determine the coordinates of the target tag j, (x_j, y_j, z_j).

3.3 Active Schemes

In contrast to the passive scheme described above for determining the RFID tag location, an active scheme is for locating a reader, with reference to a set of preinstalled passive RFID tags under a predetermined arbitrary coordinate system. We have pursued an active scheme, namely the DeB. DeB follows an iteration process to build a spherical model, which is the best fit of imperfect responses of the reference tags, such that the sphere center accurately indicates the target position. DeB is found to pinpoint a reader in the hexahedron with high accuracy. It also permits the flexible placement of reference tags. Moreover, it is RAF, avoiding the need of distance estimation according to received wireless signal strength or phase difference at the reader. Therefore, its accuracy is not materially affected by the types of readers possibly with different radiation patterns. It does not require multiple power levels, thus dodging tedious power calibration. The coordinate calculation is fast, and the system installation cost is low.

3.3.1 Localization System Description

The localization system, at which our proposed scheme aims, is illustrated in Fig. 2. A set of reference tags with known coordinates are placed on two[1] or more planes, for example, on the ceiling and the floor of the hexahedron (plus the walls to improve accuracy). The placement of reference tags can be flexible in DeB, not limited to horizontal planes but virtually anywhere inside the space, allowing more practical deployment, especially in buildings with metal frames, which seriously hinder signal propagation for RFID gear.

While both passive and active RFID tags may be deployed as reference tags, passive ones are chosen due to their lower costs (except for a large hexahedron, where active tags are indispensible for required long backscatter transmissions). Similar to the passive scheme, an arbitrary local coordinate system is assumed, as shown in Fig. 2. The reference tags are placed at known spots, with their coordinates stored either inside the tags themselves or in a database maintained by a local server. The reader is located within the hexahedron and has a fixed and suitable transmission power to activate some of those reference tags. In addition, backscatter responses emitted from activated
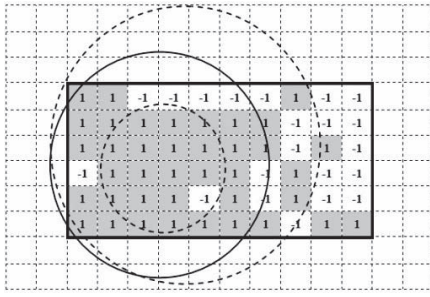
Fig. 3. Top view of reference tags under DeB, with activated (or nonactivated) tags marked by "1" (or "−1") and the solid rectangular marking hexahedron space.

Fig. 4. The histograms of reference tags along the X-axis and the Y-axis, respectively.

tags are reachable to the reader. As stated earlier, our scheme does not rely on the signal strength-based radio range estimation. Thus, it requires neither to fine-tune the transmission power nor to estimate the distance according to the received backscatter signal strength, which could result in considerable inaccuracy.

3.3.2 Overview of DeB

DeB determines directly the spherical model, which is the best fit of all activated reference tags in 3D. Its basic idea is to construct an appropriate sphere that partitions the reference tags into two classes, activated tags inside the sphere and nonactivated ones outside the sphere. If an active (or nonactivated) tag falls outside (inside) the sphere centered at the reader location, the tag is "misclassified," because it negatively guides reader location estimation. In a nutshell, DeB minimizes the total number of misclassified tags by iterative refinement in the 3D space. During an iteration, the coordinates and the radius of the sphere are rectified progressively. The refinement process repeats until the misclassification degree is below a preset threshold, yielding the estimated x, y, and z coordinates of the reader.

Unlike earlier NeM (which involves separate passes for computing the x and y coordinates on each 2D plane and for computing the z coordinate, with fewer reference tags involved during each 2D optimization phase [23]), DeB follows one single pass to compute all x, y, and z coordinates at the same time for higher accuracy, as will be demonstrated in Section 4. Additionally, as the reference tags are not read reliably, NeM calls for preprocessing tag responses so as to fill in holes (i.e., the nonactivated tags surrounded by activated tags, possibly due to false negative responses) before coordinate calculation starts [23]. By contrast, DeB requires no fill-in preprocess and is more flexible in reference tag deployment, allowing the reference tags to be placed over arbitrary planes (as opposed to only the ceiling and the floor planes under NeM).

3.3.3 Coordinates Calculation

The top view of reference tags and the sphere are illustrated in Fig. 3. The solid rectangle indicates the area of reference tags inside the hexahedron. The solid circle is the top view of a sphere that models the RFID reader coverage area. The entire space is divided into grid cells. The label inside a cell indicates its status (see Fig. 3), while the area outside the hexahedron is filled with empty cells including no reference tags. The cells with (or without) activated reference tags are marked as "1" (or "−1"). DeB follows an iterative p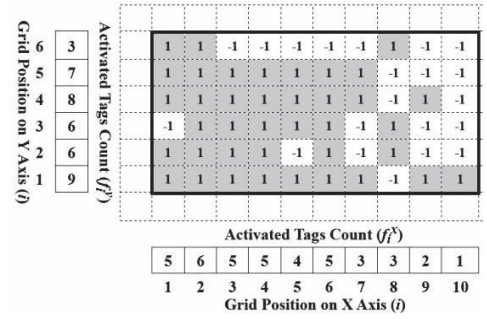rocess to lower the total distances from all misclassified reference tags to the current sphere surface progressively. This process can be done by considering the distances between the misclassified reference tags outside and inside the sphere, i.e., false positive reference tags and false negative reference tags. The former are activated reference tags outside the modeled sphere and have the positive distance values, whereas the latter are those nonactivated ones inside the modeled sphere and have the negative distance values (see Fig. 5). DeB aims to minimize the distance difference due to these two types of misclassified tags.

DeB starts with the initial values of x, y, z, and radius r, which are all obtained from the histogram of activated reference tags in each axis. As shown in Fig. 4, the histograms dictate the initial values of x, y, and z according to

$$x_{init} = \frac{\sum_{i=1}^{n_{px}} f_i^x \times i}{N_{at}}, \quad y_{init} = \frac{\sum_{i=1}^{n_{py}} f_i^y \times i}{N_{at}}, \quad z_{init} = \frac{\sum_{i=1}^{n_{pz}} f_i^z \times i}{N_{at}},$$
(3)

where n_{px}, n_{py}, and n_{pz} are the numbers of grid positions on the X-axis, the Y-axis, and the Z-axis, respectively, while f_i^x (or f_i^y or f_i^z) is the number of activated reference tags from all planes at the i position on the X (or Y or Z) axis and N_{at} is the total number of activated reference tags inside the hexahedron. For example, the initial coordinates of (x, y) in Fig. 4 are (4.49, 3.18). The initial z value can be derived in a similar way. In Fig. 2, if there are 10 (or 20) activated reference tags on the lower plane, i.e., $z = 0$ (or the upper plane, i.e., $z = H$), the initial z value is then given by $(10x0 + 20H)/(10 + 20) = 0.67H$. Note that while initial values of x, y, and z can be obtained by different expressions, those derived following (3) will guarantee convergence quickly. The initial value of r is derived by the following equation:

$$r_{init} = \max\left(\frac{x_{\max} - x_{\min}}{2}, \frac{y_{\max} - y_{\min}}{2}, \frac{z_{\max} - z_{\min}}{2}\right), \quad (4)$$

where x_{max} (or x_{min}) is the maximum (or minimum) x value among all activated tags, and $y_{\max}$, $y_{\min}$, $z_{\max}$, and $z_{\min}$ are defined similarly. The initial derived values are usually inaccurate due to those challenges outlined in Section 3.1, calling for an iterative procedure to refine them progressively. Refinement is guided by misclassified reference tags with respect to the current sphere. In Fig 5a, the two big circles (with z equal to 0 and 17) depict the intersection of the current sphere (before any refinement) with the floor and the ceiling, respectively. There exist misclassified tags. For example, the small filled circles indicate activated tags
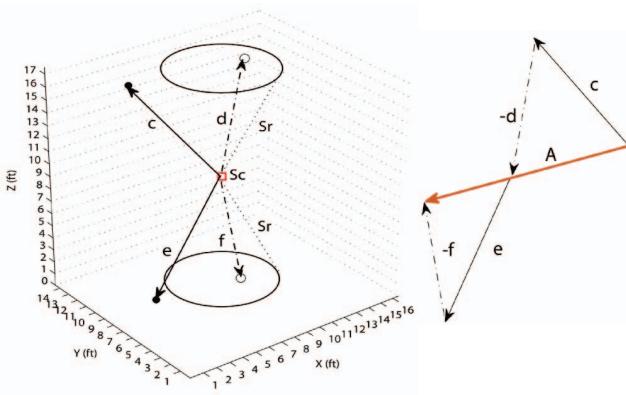
Fig. 5. Refinement in DeB, with (a) a 3D view of current sphere and misclassified tags, and (b) an involved refinement.

Fig. 6. DOI impacts under various numbers of radiation elements (k).

outside the current sphere (i.e., false positive tags) and solid vectors c and e denote their distance to the current sphere center and depicted as positive vectors in Fig. 5b, respectively. The small unfilled circles inside the sphere are nonactivated (i.e., false negative tags) and their negative distances to the current sphere center are represented by dashed vectors d and f and depicted as negative vectors in Fig. 5b, respectively.

Let S denote a 3D sphere, characterized by its center $S_C = (x_S, y_S, z_S)$ and its associated radius S_r. The sphere in iteration j, S^j is determined according to S^{j-1} and misclassified tags in the prior iteration, i.e., $S_C^j = S_C^{j-1} + C_\Delta^{j-1}$ and $S_r^j = S_r^{j-1} + r_\Delta^{j-1}$, with

$$C_\Delta^{j-1} = \frac{\sum_{i \in N_f^{j-1}} \left(\beta_i^{j-1}(P_i - S_C^{j-1}) \right)}{|N_f^{j-1}|}, \qquad (5)$$

where N_f^{j-1} is the set of misclassified tags in iteration $(j-1)$, P_i is the coordinates of Tag $T_i \in N_f^{j-1}$ and β_i^{j-1} equals

$$\beta_i^{j-1} = \begin{cases} \dfrac{l_i^{j-1} - S_r^{j-1}}{l_i^{j-1}}, & for\ S_r^{j-1} < l_i^{j-1}, \\[2mm] \dfrac{l_i^{j-1} - S_r^{j-1}}{S_r^{j-1}}, & for\ S_r^{j-1} > l_i^{j-1}, \end{cases} \qquad (6)$$

with

$$l_i^{j-1} = \sqrt{\left(x_i^{j-1} - x_S^{j-1}\right)^2 + \left(y_i^{j-1} - y_S^{j-1}\right)^2 + \left(z_i^{j-1} - z_S^{j-1}\right)^2},$$

where x_i^{j-1} (or y_i^{j-1}, or z_i^{j-1}) is the x (or y, or z) coordinate of Tag T_i and x_S^{j-1} (or y_S^{j-1}, or z_S^{j-1}) is the x (or y, or z) coordinate of sphere center S_C in iteration $(j-1)$. The essence behind (6) is as follows: If the distance from a misclassified tag (T_i) to S_C^{j-1} is larger than S_r^{j-1}, T_i is a false positive tag that should be included in the sphere, requiring that the refined sphere center S_C^j be moved toward T_i, and S_r^{j-1} be enlarged to include the tag. In contrast, if the distance is smaller, T_i is false negative one, signifying that S_C^j should be moved away from the tag, with S_r^{j-1} shrunk to exclude the tag. Accordingly, β_i^{j-1} in (5) serves as the weight due to T_i, which has a bigger impact on rectification if $|l_i^{j-1} - S_r^{j-1}|$ is larger. C_Δ^{j-1} is the aggregated impact of all misclassified tags (for example, those denoted by c, d, e, and f in Fig. 5a and c, $-d$, e, and $-f$ in Fig. 5b, with A referring to C_Δ^{j-1}), determining S_C^j.
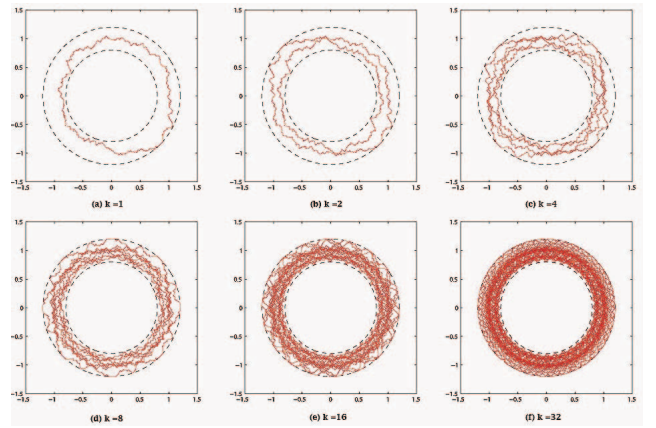
In every iteration, the sphere is enlarged or shrunk to reduce misclassified tags. The refined sphere radius amount, r_Δ^{j-1}, equals

$$r_\Delta^{j-1} = \frac{\sum_{i \in N_f^{j-1}} \left(l_i^{j-1} - S_r^{j-1} \right)}{|N_f^{j-1}|}. \qquad (7)$$

The radius adjustment process in (7) follows a similar step: a false positive (or negative) tag enlarges (or reduces) the sphere radius, for all misclassified tags in N_f^{j-1}. The refinement process for S^j repeats until it converges (i.e., when $|N_f^j|$ is smaller than a predetermined threshold). This is found to be swift, typically taking only a few iterations, as will be shown in Section 5.

3.4 Accuracy Improvement for DeB

The accuracy of DeB depends on two factors. First, it is affected by the density of reference tags. Low density tends to result in coarse granularity and high errors. To achieve high accuracy, a large number of reference tags should be deployed. The state-of-the-art RFID technology can effectively deal with the collision problem under very high tag density. In general, more reference tags yield better accuracy, naturally with a higher cost at the same time. Second, as stated in Section 3.1, signal propagation from the RFID reader does not form a sphere, due to varying signal attenuation amounts and different antenna gains in different directions. To study this problem quantitatively, we define a parameter, dubbed degree of irregularity (DOI). Given an upper bound (R_u) and a lower bound (R_l) of the reader's signal transmission range, DOI signifies the maximum variation of the reader's transmission range per unit degree change. For example, Fig. 6a shows the transmission range of a reader with DOI = 0.03 (in two dimensions). The inner circle is the lower bound, while the outer circle is the upper bound of the interrogation range. The irregular curve between them illustrates the actual transmission range of the reader over 360 degree. Clearly, DOI has a negative impact on accuracy. A larger DOI results in a more deformed circle specified by the activated reference tags, and accordingly lower accuracy.

While it is difficult to perfectly compensate the irregular antenna gains and path losses in different directions, a low-cost antenna array with multiple radiation elements may be employed to minimize the effect of DOI. (Note that

a current RFID reader may support multiple antennas; for example, each Alien Technology's ALR-9900 reader employed in our testbed has four antenna connectors [2].) The calculation of coordinates is based on all reference tags activated by the antenna array.

Figs. 6b, 6c, 6d, 6e, and 6f show the superimposed transmission range of an antenna array with 2, 4, 8, 16, and 32 radiation elements, respectively, where $R_u = 1.2$ units, $R_l = 0.8$ unit, and DOI $= 0.03$. Clearly, more radiation elements result in a set of activated tags closer to a perfect circle and accordingly more accurate results, at the expense of an increased hardware cost. We also employ an "optimized method," with calculation based only on the set of nodes which are activated by all radiation elements, to more effectively filter out irregularity. Our simulation results of the aforementioned approach for accuracy improvement are provided in the next section.

Particular challenges arise when the reader moves near a wall or a corner of a hexahedron-shaped space, due not only to abundant interrogated signals being reflected from the walls, but also to the absence of tags outside the space. As a result, those situations yield severely distorted shapes of activated reference tags, considerably hampering the accuracy of reader localization based on only those activated tags alone. To this end, an enhancement method has been developed for improving location estimation, aiming to account for those missing tags which otherwise are present if they were placed outside the room when the walls were nonexisting, known as the Enhanced DeB (EDeB). Compensated tags are virtual ones employed for helping define a less deformed sphere to arrive at better localization. The compensated tags together with those activated tags inside the room are used for computing the target location. EDeB is also applicable to situations where large objects (e.g., metal shelves) exist to block signals from the RFID reader to certain reference tags.

The way to obtain those virtual (i.e., compensated) tags starts with estimating the center position of activated tags on a given plane (be the floor or the ceiling) using DeB following (3)-(7), denoted by (x_c, y_c). The estimated center (x_c, y_c) then serves as the reference origin of a Cartesian coordinate system, called Ξ_{CC}, whose X'-axis and Y'-axis are in parallel, respectively, to the original X-axis and Y-axis of the plane, as shown in Fig. 7. Clearly, Ξ_{CC} separates activated tags into four quadrants, assuming that $x_c \neq 0$ and $y_c \neq 0$. For example, each activated tag at (x_i, y_i) in the fourth quadrant (e.g., a, b, or c), a virtual tag is obtained at location (x_v, y_v) in the second quadrant (e.g., a', b', or c'), satisfying

$$x_v = x_i \cos(\pi) - y_i \sin(\pi)$$
$$y_v = x_i \sin(\pi) - y_i \cos(\pi). \tag{8}$$

According to (8), virtual tags (x_v, y_v) outside the room are derived from activated tags (x_i, y_i) in each quadrant by rotating π to aid in pinpointing the target. As discuss earlier, the target reader is located at the point marked by a star ("☆"). Those virtual tags derived using (8) are denoted by the solid square, "■," in Fig. 7, where the new (x_c, y_c), denoted by the triangle "Δ," is seen to be closer to the center of the set of activated tags plus virtual tags than that of the set of activated tags alone. Note that EDeB is applicable for
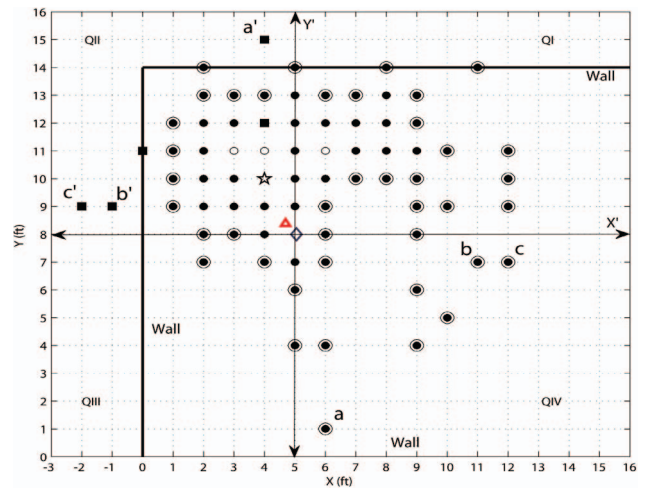

Fig. 7. The compensation process.

improving localization accuracy, provided that the target object is not located on a side wall (or at a corner). When the target is moved away from any wall (toward the room center), fewer virtual tags result, as the set of activated tags then define a better circle, calling for fewer compensated tags. In practice, the compensation process is invoked only if the target is close to a side wall, a situation which can be easily identified by examining the number of activated tags in the row (or column) just next to a wall; it is closer to the wall if the number is larger, and the compensation process is invoked when the number exceeds a threshold, say 2. Given the compensation process aims to rectify the set of tags involved in a target localization, the process may repeat after a refined center (x_c^1, y_c^1) is obtained, by viewing the new center as (x_c, y_c) and following (3)-(8) to get a new center (x_c^2, y_c^2) in the second rectification. This compensation process finishes when the distance between (x_c^i, y_c^i) in the ith iteration and (x_c^{i+1}, y_c^{i+1}) is smaller than a predetermined threshold. It is found that this refinement usually completes after a few iterations (say, 3 or less). In essence, EDeB relies on two accuracy improvement techniques: 1) *reader rotation* (to emulate an antenna array with k radiation elements, by rotating 360 degree/k in each step) to deal with DOI and 2) tag compensation to deal with "wall adversary." Experimental results of EDeB will be demonstrated in Section 5.2.

4 SIMULATION RESULTS

We carry out extensive simulations by using Matlab [12] and Java codes to evaluate our proposed 3D RFID positioning schemes. In particular, we study the impact of several parameters of interest, such as the radio propagation irregularity, the number of radiation elements of the antenna array, and the reference node density, which may dictate the accuracy of our passive and active schemes. We have simulated a hexahedron of the size of a typical container (about $40' \times 8' \times 8'$).

4.1 Passive Scheme

As we have discussed in Section 3.2, a set of reference tags and readers need to be deployed on the floor or the ceiling of the hexahedron for the passive scheme. In our simulation, $N = 12$ readers are deployed by default. The density of
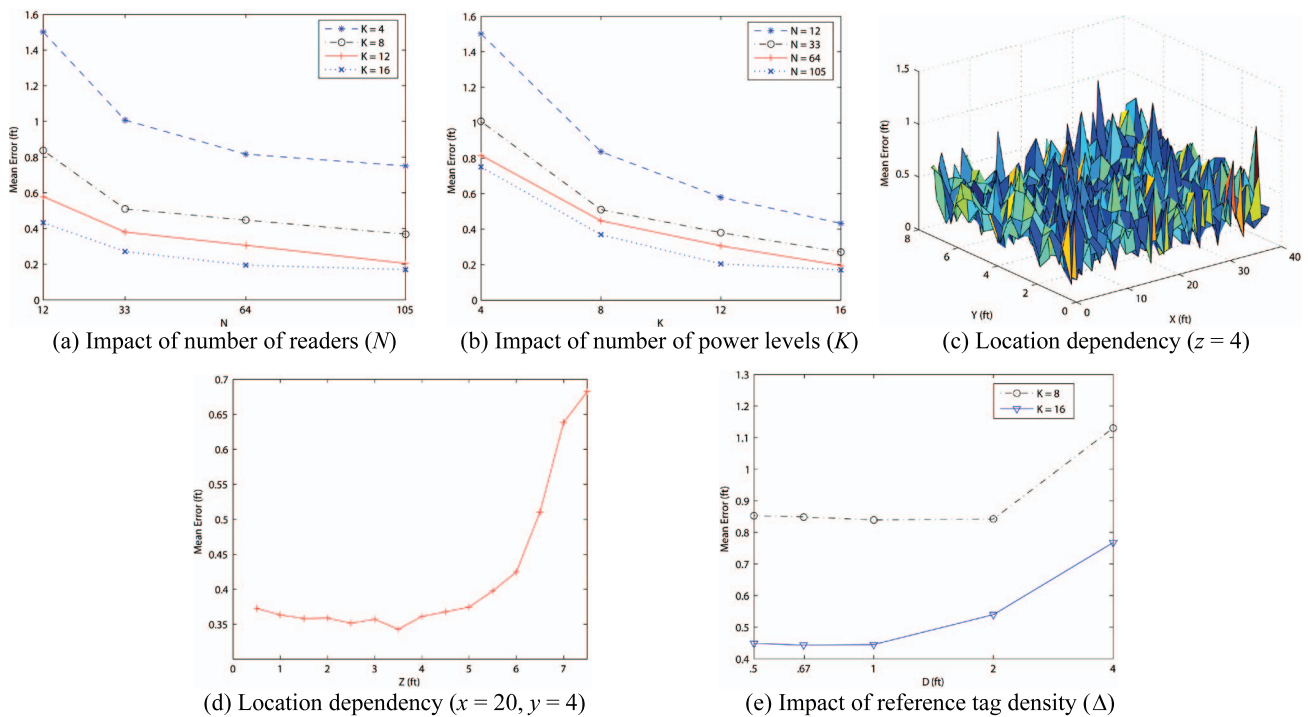
(a) Impact of number of readers (N)

(b) Impact of number of power levels (K)

(c) Location dependency ($z = 4$)

(d) Location dependency ($x = 20$, $y = 4$)

(e) Impact of reference tag density (Δ)

Fig. 8. Simulation results under the passive scheme.

the reference tags is represented by a parameter Δ, which is the distance between two adjacent reference tags, with Δ equal to 1 ft by default. Each reader has K transmission power levels with a maximum transmission range of 16 feet. We assume the transmission power levels are calibrated so that there is a linearly increasing response range with the increase of power level, to improve the accuracy. In other words, the transmission range per power level is $16/K$ feet. We vary the values of N, Δ, and K to observe their impacts on the accuracy of the passive scheme. The error is defined as the absolute difference between the actual coordinates of (x, y, z) and the calculated coordinates of target objects, (x_c, y_c, z_c), as expressed by

$$Error = \sqrt{(x - x_c)^2 + (y - y_c)^2 + (z - z_c)^2}.$$

The results are the average of 2,560 sample points distributed uniformly in the hexahedron.

We have observed from our simulation that there is a tradeoff between the accuracy and the cost in the implementation of the passive scheme. We first study the impact of the number of reference readers (N). As can be seen in Fig. 8a, the errors decrease with more readers deployed, because more readers result in a more accurate error objective function (i.e., with more terms in (1)). At the same time, however, deploying more readers clearly increases the system cost and leads to a higher computing complexity and longer time to locate the target.

Besides the number of readers, the number of power levels (K) available to each reader is usually a dominating factor on the accuracy of the passive scheme. Our results show that more accurate coordinates are yielded with more power levels (see Fig. 8b, with K up to 16). This is reasonable, because a larger K results in a finer increase in the readers' transmission power and, thus, more accurate estimation of distances from the target tag to the readers.

However, the reader with many power levels is usually unavailable off-shelf or prohibitively expensive.

Figs. 8c and 8d show the impact of target locations on the accuracy of the passive scheme. It is observed that the accuracy of x and y is insensitive to the location of the target. The errors vary only marginally with the location. At the same time, the error of z is not affected much by the location when the target is below 5 feet. While the target becomes very close to the ceiling, the error of z increases significantly because the relative error becomes high.

In addition, we observe that the density of reference tags has less impact on accuracy compared with N and K (see Fig. 8e). This is because the density of the reference tags is often sufficiently high, leading to a much finer granularity, compared with the readers' transmission power levels. In particular, Δ does not noticeably affect accuracy when $\Delta \leq 16/K$, because, with the reference tag density so high, the power level granularity completely dominates the errors.

4.2 Active Scheme

To employ the proposed localization scheme, a set of reference tags are placed at known coordinates on the floor and the ceiling of the hexahedron. Similar to the simulations for the passive scheme, the density of the reference tags is represented by Δ, which equals 1 foot. The target RFID reader is located inside the hexahedron and has a fixed transmission power, which results in $R_u = 7.2$ ft and $R_l = 4.8$ ft (i.e., the upper and the lower bounds of reader's transmission range). The default value of DOI is 0.03. The results are based on an antenna with four (4) radiation elements, unless specified otherwise.

To characterize DeB accuracy, we compare the simulation results of DeB with those of NeM in all three different approaches for selecting reference tags: SCM, IBM, and FBM [23]. In addition, the "optimized" scheme discussed in

(a) Impact of DOI

(b) Impact of radiation elements (k)

(c) Impact of reference tag density (Δ)

(d) Execution time versus the number of involved reference tags (n)

(e) Location dependency on X- and Y-coordinates with $z = 4$
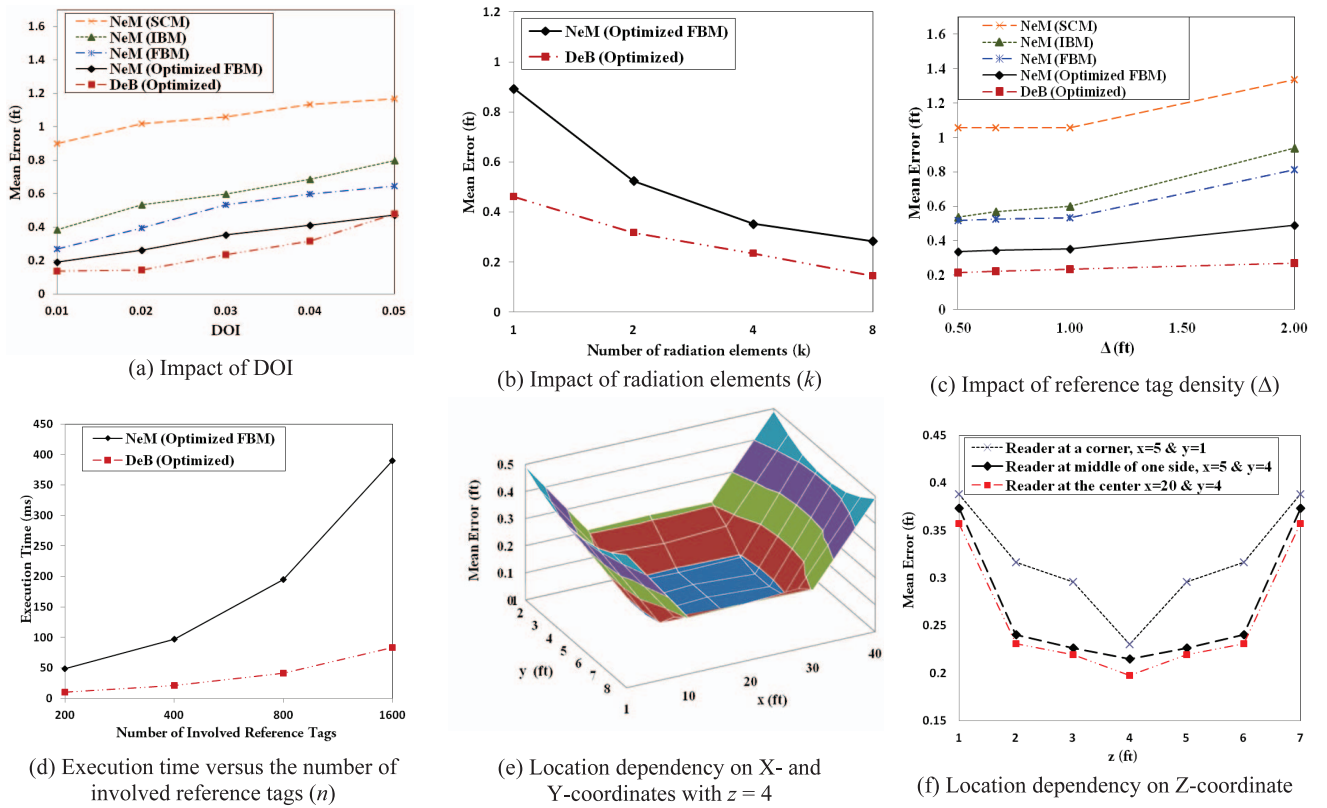
(f) Location dependency on Z-coordinate

Fig. 9. Simulation results under DeB and NeM active schemes.

Section 3.4 was incorporated to effectively utilize all radiation elements for compensating DOI, on top of DeB and of NeM with the FBM. We vary Δ, DOI, and the number of elements k to observe their impacts on the accuracy under DeB and under NeM. The impact of DOI on accuracy for $\Delta = 1.0$ ft is depicted in Fig. 9a, where the errors are seen to increase monotonically with DOI, because higher DOI results in a more deformed sphere (under DeB) or circle (under NeM) of the activated reference tags and accordingly larger errors in finding the target coordinates. NeM (with optimized FBM) is more accurate than other NeM methods, able to locate the target with errors less than 0.5 ft even when DOI is high. NeM (with SCM), on the other hand, results in the largest error, because it is heavily affected by the partial circles when the target is near a hexahedron side or corner. As expected, DeB (which is "optimized," i.e., its calculation is based only on the set of nodes that are activated by all k radiation elements) achieves the best accuracy and is robust to the increase of DOI, because it handles all misclassified reference tags by 3D optimization effectively.

Employing more radiation elements can effectively reduce the negative impact of DOI, as illustrated in Fig. 9b, where the results of DeB and NeM (with optimized FBM) under various numbers of radiation elements are shown. The errors are the largest under one antenna (i.e., $k = 1$), and they are reduced sharply when the antenna array deployed has two and four radiation elements. More radiation elements yield smaller errors, because those activated tags better construct a sphere, thereby yielding more accurate target coordinates. DeB outperforms NeM consistently for any given k.

The density of the reference tags (Δ) also affects achievable accuracy. As also demonstrated in Fig. 9c, a higher density (i.e., smaller Δ) tends to result in smaller errors. When Δ becomes ≤ 1 ft, however, it has an insignificant impact on the accuracy of any scheme. This is because, for $\Delta \leq 1$ ft, the density of reference tags is no longer a dominating factor, as the errors are then introduced mainly by DOI. Clearly, DeB outperforms NeM for any Δ, achieving an error of some 0.2 ft only for $\Delta = 1.0$ ft, in comparison to more than 0.3 ft under the best NeM, i.e., NeM (with optimized FBM). In addition, the gap widens as Δ grows.

The execution times (in ms) of location identification schemes versus the number of involved reference tags (n) are depicted in Fig. 9d, where the density of the reference tags (Δ) is fixed at 1.0 ft and n includes all activated tags plus all nonactivated tags located within the reader antenna range. When the number of involved tags (n) rises, the execution time grows accordingly for every identification scheme, as expected. The proposed DeB scheme enjoys the time complexity of $O(n)$ in the presence of n involved tags, exhibiting far smaller execution times when compared with the earlier NeM counterpart (which requires two rounds of 2D optimization on the ceiling and the floor planes separately, followed by z coordinate calculation [23]). Given $n = 1,600$, for example, DeB run on a laptop takes only 83 ms, in contrast to some 400 ms (ignoring the time for preprocessing activated tags) under NeM, as illustrated in Fig. 9d. It should be noted that the number of involved reference tags (n) depends solely on the reader antenna range and the tag density (Δ), irrespective of the total number of tags deployed or the hexahedron size. The

proposed DeB smartly outperforms NeM in both identification accuracy and speed, suitable for real-time applications.

Figs. 9e and 9f show the errors of DeB at various locations in the hexahedron. The highest accuracy is observed when the target is at the center of the hexahedron, i.e., $x = 20$ and $y = 4$ for $z = 4$, where the coordinate error approaches 0.2 ft. When the target RFID reader moves closer to a hexahedron corner, the errors grow monotonically because the circles or spheres formed by those activated reference tags suffer from more distortion. This calls for an enhancement method to deal with those situations with pronounced localization inaccuracy, and such a method will be detailed in the next section.

In addition to its fast localization and high accuracy, the proposed DeB scheme is readily applicable in practice because it employs only passive tags, whose price may soon drop to several cents apiece. Currently, the passive tags adopted for our experimental study (i.e., the Alien Squiggle tags) cost less than 15¢/each (for a roll of 10,000 at $1,488.00). The DeB identification time for a huge room (say, sized 99 ft by 49 ft by H, where H is the reader antenna range) with 10,000 deployed tags remains no more than 83 ms as long as $n \leq 1,600$ (see Fig. 9d). Consequently, a DeB-based RFID positioning system can be established with a fairly low cost while achieving high reader localization of any place inside a 3D hexahedron.

5 EXPERIMENTAL EVALUATION

5.1 Experimental Setup

To further investigate the effectiveness of our proposed 3D positioning schemes, we have conducted experiments by using the Alien RFID kits [1], [2], including an ALR-9900 RFID reader and ALN-9540 Squiggle tags. Our experiments were done in the realistic environment of 16 ft long, 14 ft wide, and 17 ft high. The ALR-9900 reader connects via the TCP/IP port, on which basic web-based utility software is run to control the reader (e.g., to find a suitable transmission power level) and the Java program is run to obtain the results (e.g., to acquire the ID of responding tags), needed for our 3D positioning schemes. A circularly polarized antenna is attached to the reader, which supports up to four antennas. A photo of our experimental setup is shown in Fig. 10, where the white box is a reader's antenna attached to the red box, which is an RFID reader. The reference tags are the small rectangles placed on the middle of each square ceiling board. We carried out experiments using ALN-9540 tags and ALR-9900 reader attached with an antenna, as mention earlier. Given that the reader's antenna has coverage area far beyond the room under its regular transmission power, our experiments lowered the antenna's transmission power to -15 dbm so as to ensure that some parts of the sphere surface are located inside the target room.

Without loss of generality, an arbitrary coordinate system is assumed, with its origin at the reader's antenna in each experimental setup. The reference tags are put at grid points across the ceiling and on the floor, with the distance between two adjacent grid points equal to 1 ft, as depicted in Fig. 11. In the figure, an activated tag is denoted by a small circle with a solid center, and those on the floor are easier to be visualized (than those on the ceiling), with

Fig. 10. The experimental setup in the real environment.

the actual reader position denoted by a star and the calculated reader locations according to DeB and NeM schemes marked under each situation.

As described in Section 3.4, the reader antenna suffers from DOI, which can be mitigated using the antenna array. Without a suitable antenna array at hand, we emulated the effect of an antenna array (with k radiation elements) via rotating the reader antenna k times each by $(360/k)$ degree during every experiment to suppress DOI. A larger k tends to yields a better shaped sphere those activated tags, thus higher accuracy in locating the target object.

5.2 Experimental Results and Discussion

Six sets of experimental data are presented in Fig. 11 for evaluating the accuracy of DeB and NeM, under various target positions and different k values. More specifically, we have carried out experiments when the target reader antenna is situated at the center (with $x = 8.5, y = 7.5, z = 8.5$), close to a sidewall (with $x = 8.5, y = 4.0, z = 8.5$) and to a corner (with $x = 4.0, y = 10.0, z = 8.5$) of the room. We vary k to be 1 and 4. When $k = 4$, the reader's antenna was rotated by 90 degree for four times, and those activated tags with respect to each antenna orientation were aggregated together for computing the reader location. This process can also be done in one step without rotation by using four antenna arrays as discuss in Section 3.4 to collect the tag information at once. In Fig. 11, the target reader is located at the point marked by a star ("☆"), whereas the calculated positions under DeB (or NeM) is denoted by "◇" (or "+").

If the target reader is moved toward a corner or a sidewall of the room, computed coordinates exhibit higher errors due mainly to fewer tags being activated because no tags are outside the room, and also to rising interferences caused by heavier reflection from the walls, as stated earlier and confirmed in Figs. 11c, 11d, 11e, and 11f. To deal with this "wall adversary," EDeB was introduced in Section 3.4
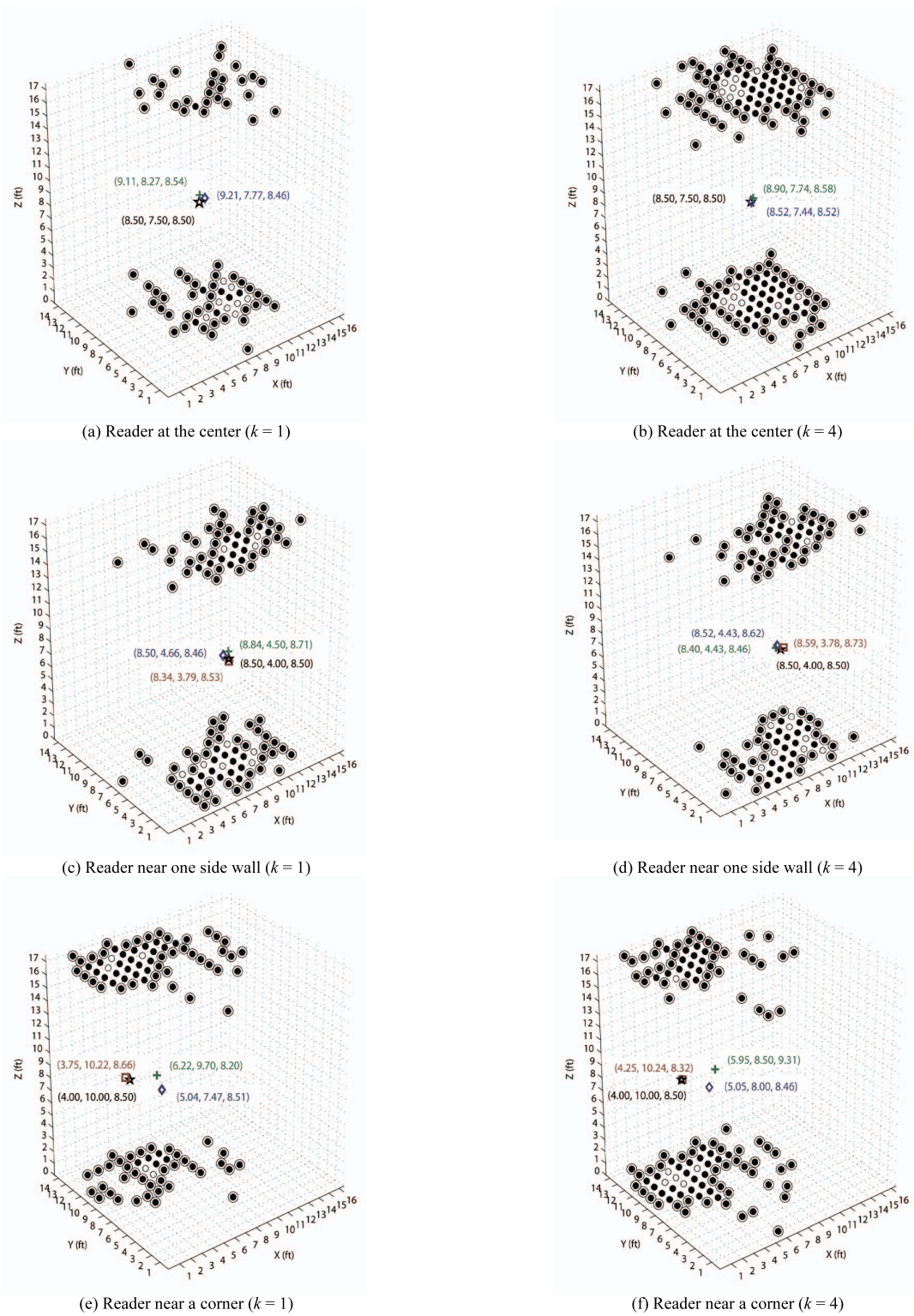
(a) Reader at the center ($k = 1$)

(b) Reader at the center ($k = 4$)

(c) Reader near one side wall ($k = 1$)

(d) Reader near one side wall ($k = 4$)

(e) Reader near a corner ($k = 1$)

(f) Reader near a corner ($k = 4$)

Fig. 11. The experimental results, with actual reader position indicated by the star, "☆". The diamond, "◇" (or the cross "+"), denotes the position estimated by DeB (or NeM) and the square "□" denotes the result under EDeB calculation with the accuracy enhancement process applied.

to enhance the accuracy through a compensation process which accounts for those "missing" tags outside the room. Experimental results under EDeB are also illustrated in Fig. 11, as marked by "□". When the reader is situated in the room center with $k = 1$, DeB scheme works to locate the target accurately, as illustrated in Fig. 11a, exhibiting an error of 0.76 ft (which is better than 0.98 ft under NeM).

Utilizing the accumulated tag responses after $k = 4$ rotations (each by 90 degree), both DeB and NeM improve coordinate accuracy, as shown in Fig 11b. Specifically, the error then stands at 0.07 ft under DeB to enjoy 91 percent improvement over $k = 1$, whereas the error drops to 0.47 ft under NeM. In this case, DeB is far more accurate than its NeM counterpart.
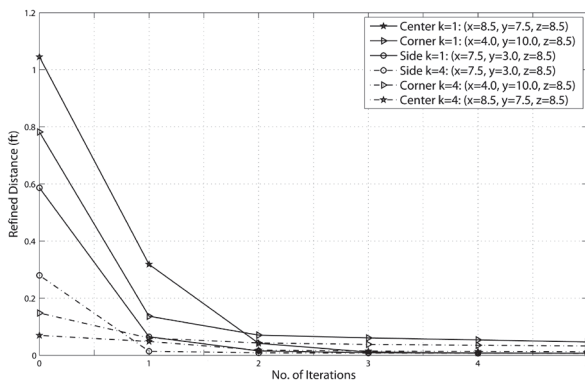
Fig. 12. RD (i.e., A shown in Fig. 5b in ft) from (5) versus number of iterations under DeB.

Fig. 13. Localization error (in ft) versus number of iterations under EDeB.

When the reader is moved toward a side of the room, the accuracy of DeB deteriorates, as demonstrated in Figs. 11c and 11d. In addition, the benefit from an antenna array (of $k = 4$) drops, with the calculated errors equal to 0.45 ft under $k = 4$. On the other hand, EDeB brings down the error to roughly 0.3 ft for both $k = 1$ and $k = 4$, as denoted by "□". Apparently, tag compensation is more effective in accuracy improvement in this situation, as expected, because it is aimed to handle "wall adversary." The localization errors rise noticeably when the reader is moved toward a corner of the room, as depicted in Figs. 11e and 11f, with the errors approaching 2.2 ft to 2.7 ft even for $k = 4$ under both DeB and NeM. These large errors are due to severe "wall advisory," which has to be dealt with using tag compensation. Indeed, EDeB boosts localization accuracy significantly, giving rise to errors below 0.4 ft (representing accuracy improvement more than 80 percent) under both $k = 1$ and $k = 4$, as demonstrated in Figs. 11e and 11f. Given error amounts are comparable under $k = 1$ and $k = 4$, reader rotation offers limited alleviation for wall advisory, and tag compensation is indispensable. The tag compensation process repeats to arrive at more accurate target coordinates progressively. Progressive iterations are found to lower refined distance (RD) monotonically, as depicted in Fig. 12, where RD refers to as the sum of the distance between each misclassified tag and the surface of the defined sphere calculated from (5).

Misclassified tags fall into two categories: the false positive and false negative activated tags, with the former (or the latter) ones yielding positive (or negative) distance values in calculating RD. According to the curves in Fig. 12, the RDs, or "A" shown in Fig. 5b under DeB, decrease quickly, and they drop to negligible amounts in a few iterations, for all of our experimental scenarios considered. The computation times taken by this compensation process are small, involving some 20 ms (or 40 ms) only if the target is at the center (or near a wall), when executed on a Dell Optiplex GX745 desktop machine with Core2 CPU @2.40 GHz and 3 GB of memory.

Localization error versus the number of iterations under EDeB is illustrated in Fig. 13. Four scenarios are included in the figure, including the target located close to a wall and to a corner with $k = 1$ and $k = 4$. Tag compensation lowers the computed errors effectively, greatly enhancing localization accuracy. Under the worst scenario considered (for the
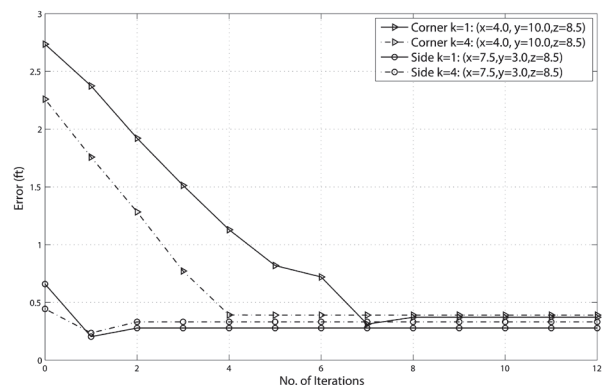
target near a corner with $k = 1$), tag compensation is shown to bring the error down to about 0.4 ft in eight iterations, resulting in accuracy improvement of some 86 percent.

6   CONCLUSION

We have considered and contrasted two RFID-based 3D localization schemes, namely, the passive scheme and the active scheme aiming to locate a target object in 3D space. Both schemes are RAF (i.e., distance estimation based on signal strength is not require), thus exhibiting accuracy levels independent of reader types (with varying radiation patterns). In the passive scheme, we locate an RFID tag, which is attached to the target object using RFID tags and readers as the reference points. Under the active scheme, we propose the DeB scheme for inexpensively and quickly locating either a mobile person or robot who wears an RFID reader or an object approached by an RFID reader in a 3D space. Deemed the very first RAF 3D localization without involving other devices or sensors in support of high accuracy, the active scheme employs a set of RFID tags with known locations as references to pinpoint a reader operating in one fixed power level as the target object.

We have carried out analyses, extensive simulations, and testbed experiments to evaluate the proposed schemes under various system parameters, including the DOI, the number of radiation elements of the antenna array, and the reference tag density. Our results show that both schemes are effective, with active schemes outperform the passive one. They also demonstrate that the proposed active scheme (DeB) clearly prevails over its earlier counterpart (i.e., NeM [23]) in both identification accuracy and speed, suitable for real-time applications. Furthermore, EDeB is developed for accuracy improvement, often locating an RFID reader dramatically better, in particular when it is close to a side or corner of a 3D hexahedron.

REFERENCES

[1] Alien Technology Corp., "ALN-9540 Squiggle Inlay: Product Overview," http://www.alientechnology.com/docs/products/DS_ALN_9540.pdf, Aug. 2008.

[2] Alien Technology Corp., "ALR-9900 Enterprise RFID Reader: Product Overview," http://www.alientechnology.com/docs/products/DS_ALR_9900+pdf, Mar. 2010.

[3] A. Almaaitah et al., "3D Passive Tag Localization Schemes for Indoor RFID Applications," *Proc. IEEE Int'l Conf. Comm. (ICC '10),* pp. 1-5, May 2010.

[4] M. Baglietto et al., "A Multi-robot Coordination System Based on RFID Technology," *Proc. 14th Int'l Conf. Advanced Robotics (ICAR '09),* pp. 1-6, June 2009.

[5] R. Bridgelall, M.W. Duron, and M.J. Strzelezyk, "Object Location System and Method Using RFID," US Patent no. 7,119,738, Oct. 2006.

[6] D. Hahnel et al., "Mapping and Localization with RFID Technology," *Proc. IEEE Int'l Conf. Robotics and Automation,* pp. 1015-1020, Apr. 2004.

[7] T. He et al., "Range-Free Localization Schemes for Large Scale Sensor Networks," *Proc. ACM MobiCom '03,* pp. 81-95, Sept. 2003.

[8] C. Hekimian-Williams et al., "Accurate Localization of RFID Tags Using Phase Difference," *Proc. IEEE Fifth Ann. Int'l Conf. RFID,* pp. 89-96, Apr. 2010.

[9] J. Hightower, R. Want, and G. Borriello, "SpotON: An Indoor 3D Location Sensing Technology Based on RF Signal Strength," Technical Report UW CSE #2000-02-02, Univ. of Washington, Feb. 2000.

[10] M. Li and Y. Liu, "Rendered Path: Range-Free Localization in Anisotropic Sensor Networks with Holes," *Proc. ACM MobiCom '07,* pp. 51-62, Sept. 2007.

[11] H. Liu et al., "Survey of Wireless Indoor Positioning Techniques and Systems," *IEEE Trans. System, Man, and Cybernetics,* vol. 37, no. 6, pp. 1067-1080, Nov. 2007.

[12] Matlab. http://www.mathworks.com, 2013.

[13] M.A. Mehmood, L. Kulik, and E. Tanin, "Autonomous Navigation of Mobile Agents Using RFID-Enabled Space Partitions," *Proc. 16th ACM Int'l Conf. Advances in Geographic Information Systems,* article 21, Nov. 2008.

[14] A. Milella et al., "RFID Tag Bearing Estimation for Mobile Robot Localization," *Proc. 14th Int'l Conf. Advanced Robotics (ICAR '09),* pp. 1-6, June 2009.

[15] V.P. Munishwar et al., "On the Accuracy of RFID-Based Localization in a Mobile Wireless Network Testbed," *Proc. IEEE Fifth Workshop Pervasive Wireless Network (PWN '09),* pp. 1-6, Mar. 2009.

[16] J.A. Nelder and R. Mead, "A Simplex Method for Function Minimization," *The Computer J.,* vol. 7, no. 4, pp. 308-313, 1965.

[17] L.M. Ni et al., "LANDMARC: Indoor Location Sensing Using Active RFID," *Proc. IEEE Conf. Pervasive Computing and Comm. (PerCom '03),* pp. 407-415, Mar. 2003.

[18] N.B. Priyantha, A. Chakraborty, and H. Balakrishnan, "The Cricket Location-Support System," *Proc. ACM MobiCom,* pp. 32-43, Aug. 2000.

[19] Y. Raoui et al., "RFID-Based Topological and Metrical Self-Localization in a Structured Environment," *Proc. 14th Int'l Conf. Advanced Robotics (ICAR '09),* June 2009.

[20] T. Sanpechuda and L. Kovavisaruch, "A Review of RFID Localization: Applications and Techniques," *Proc. Fifth Int'l Conf. Electrical Eng. and Information Techniques,* pp. 769-772, 2008.

[21] SkyeTek Inc., "SkyeModule M1-Mini," http://www.skyetek.com/ProductsServices/EmbeddedRFIDReaders/SkyeModuleM1mini/tabid/338/Default.aspx, 2005.

[22] T. Wada et al., "A Novel Localization Scheme for Passive RFID Tags; Communication Range Recognition (CRR)," *Proc. IEEE Fourth Ann. Int'l Conf. RFID,* pp. 163-169, Apr. 2010.

[23] C. Wang, H. Wu, and N.-F. Tzeng, "RFID-Based 3-D Positioning Schemes," *Proc. IEEE INFOCOM '07,* pp. 1235-1243, May 2007.

[24] R. Want et al., "The Active Badge Location System," *ACM Trans. Information Systems,* vol. 10, no. 1, pp. 91-102, Oct. 1992.

[25] P. Wilson, D. Prashanth, and H. Aghajan, "Utilizing RFID Signaling Scheme for Localization of Stationary Objects and Speed Estimation of Mobile Objects," *Proc. IEEE Int'l Conf. RFID,* pp. 94-99, Mar. 2007.

[26] H. Wu, C. Wang, and N.-F. Tzeng, "Novel Self-Configurable Positioning Technique for Multi-Hop Wireless Networks," *IEEE/ACM Trans. Networking,* vol. 13, no. 3, pp. 609-621, June 2005.

[27] K. Yamano et al., "Self-Localization of Mobile Robots with RFID System by Using Support Vector Machine," *Proc. IEEE/RSJ Int'l Conf. Intelligent Robots and Systems,* pp. 3756-3761, Sept./Oct. 2004.

Jullawadee Maneesilp received the bachelor's and master's of engineering degrees in computer engineering from Kasetsart University, Bangkok, Thailand in 1999 and 2002, respectively, and the master's of science and the PhD degrees in computer science from the University of Louisiana at Lafayette, in 2007 and 2011, respectively. She received the Royal Thai Government Scholarship in 2005 to pursue the master's and the doctoral degrees in computer science. Currently, she works in the Pollution Control Department, Ministry of Natural Resources and Environment, Bangkok, Thailand, with research interest in the areas of network security and wireless sensor network technology.

Chong Wang received the BS degree in physics from Fudan University, Shanghai, China, in 1992, and the MS and PhD degrees in computer science from the University of Louisiana at Lafayette, in 2000 and 2008, respectively. His research interests include radio frequency identification (RFID) systems and wireless sensor networks.

Hongyi Wu (M'02) received the BS degree in scientific instruments from Zhejiang University, Hangzhou, China, in 1996, and the MS degree in electrical engineering and PhD degree in computer science from the State University of New York (SUNY) at Buffalo in 2000 and 2002, respectively. He is currently an associate professor with the Center for Advanced Computer Studies, University of Louisiana at Lafayette. His research spans delay-tolerant networks, radio frequency identification (RFID) systems, wireless sensor networks, and integrated heterogeneous wireless systems. He received the National Science Foundation (NSF) CAREER Award in 2004 and the University Foundation Distinguished Professor Award in 2011. He is a member of the IEEE.

Nian-Feng Tzeng (M'86-SM'92-F'10) received the PhD degree in computer science from the University of Illinois at Urbana-Champaign. Since 1987, he has been with Center for Advanced Computer Studies, the University of Louisiana at Lafayette, where he is currently a professor. He was on the editorial board of the *IEEE Transactions on Parallel and Distributed Systems*, 1998-2001, and on the editorial board of the *IEEE Transactions on Computers*, 1994-1998. He is on the editorial board of *Journal of Information Science and Engineering* (JISE, published by Academia Sinica, Taiwan). He served as a distinguished visitor of the IEEE Computer Society, 1994-1997, and was the chair of Technical Committee on Distributed Processing, the IEEE Computer Society, from 1999 to 2002. His current research interest is in the areas of computer communications and networks, high-performance computer systems, parallel and distributed processing, and fault-tolerant computing. He is the recipient of the outstanding paper award of the 10th International Conference on Distributed Computing Systems, May 1990, and also of the University Foundation Distinguished Professor Award in 1997. He is a fellow of the IEEE and the IEEE Computer Society.